Applied Geochemistry 158 (2023) 105800

Contents lists available at ScienceDirect

Applied Geochemistry

journal homepage: www.elsevier.com/locate/apgeochem

# Remediation of acid mine drainage and immobilization of rare earth elements: Comparison between natural and residual alkaline materials

Dileesha Jayahansani Kotte-Hewa [a,c,*], Delphine Durce [a], Sonia Salah [a], Carlos Ruiz Cánovas [b], Erik Smolders [c]

[a] Belgian Nuclear Research Centre, SCK CEN, Boeretang 200, Mol, 2400 Belgium
[b] Department of Earth Sciences & Research Center on Natural Resources, Health and the Environment, University of Huelva, Campus "El Carmen", E-21071, Huelva, Spain
[c] KU Leuven, Department of Soil and Water Management, Kasteelpark Arenberg 20, 3001, Heverlee, Belgium

ARTICLE INFO

*Keywords:*
Acid mine water remediation
Passive treatment systems
Waste products
Blast furnace slag
Biomass ash
Rare earth elements

ABSTRACT

Acid mine drainage (AMD) is a well-known source of toxic trace metals in freshwaters. Traditional passive treatment systems rely on AMD neutralization with limestone and removal of most common toxic transition metals such as Cu and Zn with little attention to rare earth elements (REE). Alkaline waste materials now receive increasing attention as low cost AMD treatment alternatives in the circular economy. This study was set up to identify the efficiency of alkaline waste materials remediating AMD and scavenging REE in addition to other toxic trace elements. An AMD sample was collected from a lixiviate coming from pyrite heaps in the Iberian Pyrite Belt (pH = 1.8, 30 μM ∑REY). The sample was treated with either blast furnace slag (BFS) generated during smelting of iron ore in a blast furnace or biomass ashes (BA) derived from combustion of biomass, thereby using analytical grade $CaCO_3$, and NaOH as reference products. The batch alkalinization experiments were conducted by adding each alkaline material at an amount to obtain an equal pH to ≈6.5. The required amounts of the products were NaOH < $CaCO_3$<BFS < BA in line with their acid neutralizing capacities. The largest removal of sulfate from water was obtained in the $CaCO_3$ treatment suggesting gypsum precipitation which was lower with BA and BFS and virtually absent with NaOH, these trends were confirmed by SEM-EDX and XRD. Both BFS and BA removed more Fe than $CaCO_3$ and NaOH. The REE elements were well removed by all treatments (>99%) and the remaining REE concentrations in the solutions were clearly lower than values for Cu and Zn. The Zn and Cu removals were not consistently high enough (except with NaOH) to meet environmental limits in the discharge waters. The largest efficiency for REE removals was obtained with $CaCO_3$. Indirect evidence here suggests that gypsum is a better host for the trivalent REE than Fe(III) minerals in the precipitates. The ionic radii of trivalent REE are more similar to $Ca^{2+}$ than to $Fe^{3+}$, explaining the better potential of gypsum as REE host. This study showed also the potential of BFS as alkaline agent for the remediation of AMD in terms of its higher alkalinity generation potential as compared to BA, thus making BA less promising than BFS.

## 1. Introduction

Acid mine drainage (AMD) is a major source of metal contamination of freshwaters. Its generation is mainly induced by the oxidation of sulphidic ores i.e. pyrite ($FeS_2$) during mining and mineral exploitations. This acid flow then facilitates dissolution of elements contained in sulfides as impurities such as Cu, Zn, Cd, As and Pb. In addition, the high acidity released also leads to the dissolution of other elements, i.e. Al, Ca, Mg, Na, K and rare earth elements (REE) contained in the host rocks surrounding the sulfides. The low pH increases the solubility and mobility of REE, which are commonly found in AMDs in concentrations several orders of magnitude higher than those found in natural freshwater bodies (Ayora et al., 2016; Noack et al., 2014; Wang et al., 2021; Zänker et al., 2003; León et al., 2021). If left untreated, AMD may contaminate aquatic and terrestrial environments even after closing of the mining activities (Doye and Duchesne, 2003; Akinwekomi et al., 2016; Duraes et al., 2017; Ferreira da Silva et al., 2009; Masindi, 2017; Perez-Lopez et al., 2011; Ruehl and Hiibel, 2020; Sheoran, 2006;

* Corresponding author. Belgian Nuclear Research Centre, SCK CEN, Boeretang 200, Mol, 2400, Belgium.
*E-mail address:* dileesha.kotte.hewa@sckcen.be (D.J. Kotte-Hewa).

https://doi.org/10.1016/j.apgeochem.2023.105800
Received 11 July 2023; Received in revised form 21 September 2023; Accepted 26 September 2023
Available online 27 September 2023

Totsche et al., 2006; Turingan et al., 2022). The historical mining area stretching from southwest of Spain to Portugal known as the Iberian Pyrite Belt (IPB) is one example illustrating the severity of AMD generation. The IPB contains one of the largest concentrations of massive sulfide deposits in the world. More than 100 abandoned mines present in the IPB have been collectively contributing to this pollution problem for decades (Duraes et al., 2017; Gonzalez et al., 2020; Orden et al., 2021; Soyol-Erdene et al., 2018).

The AMD can be treated by using either active treatment systems (ATS) or passive treatment systems (PTS) (Ben Ali et al., 2019). ATS, which involve a water treatment plant, are a prerequisite of active mining operations which have to comply a strict control of the final effluent quality before being released in the environment (Turingan et al., 2022). PTS are generally used for the rehabilitation of closed and abandoned mine sites. ATS are based on the continuous addition of chemicals (i.e., NaOH) and use of electricity (Macías et al., 2017; Skousen et al., 2019; Cánovas et al., 2020), while PTS do not require this continuous addition and employ naturally available energy sources i.e., gravity flow and natural oxidation. Natural material, such as limestone, or even constructed wetlands (Orden et al., 2021; Caraballo et al., 2009; Hengen et al., 2014; Macias et al., 2012a) are used in PTS for remediation. The PTS require, therefore, less maintenance and lower energy costs than ATS (Perez-Lopez et al., 2011; Ruehl and Hiibel, 2020; Turingan et al., 2022; Orden et al., 2021; Bernier, 2005; Ness et al., 2014; Sheridan et al., 2013). Some PTS, such as the Dispersed Alkaline Substrate (DAS) technology which is in use at the Mine Esperanza and Mine Concepción in the IPB (Orden et al., 2021) rely on the pH neutralization and subsequent metal precipitation using alkaline materials with limestone ($CaCO_3$) mainly for trivalent metal precipitation (i.e. $Fe^{3+}$ and $Al^{3+}$) and complemented by an additional treatment step with MgO, for divalent metal precipitation (i.e. $Cu^{2+}$, $Zn^{2+}$, $Mn^{2+}$etc.) (Caraballo et al., 2009). This neutralization is performed in tanks filled with a mixture of coarse materials (i.e., wood chips) and alkaline materials to prevent the clogging problems related to Fe precipitation commonly observed in PTS applied to AMD (Orden et al., 2021). Inside the limestone-DAS PTS, AMD flows down in a vertical direction and gets in contact with $CaCO_3$. Upon contact, $CaCO_3$ starts to dissolve and generates alkalinity (Lozano et al., 2019a). Along this alkalinization process, between pH 3–4.5, Fe starts to precipitate as poorly crystalline iron oxyhydroxysulphate (i.e. schwertmannite ($Fe_8O_8(SO_4)_x(OH)_y.nH_2O$, where x = 1.4–1.5, y = 5.0–5.2)) (Lozano et al., 2019a). Then, when the pH further increases to pH 4.5–6, Al starts to precipitate. Lozano et al. (2020) and Sánchez-España et al. (2011) identified microcrystalline aluminium oxyhydroxysulphate (i.e. basaluminite ($Al_4(SO_4)(OH)_{10}.15H_2O$)) as the main formed Al phase (Lozano et al., 2020a; Sánchez-España et al., 2011). Ferrihydrite, a low crystallinity Fe (III) oxide ($Fe(OH)_3$) is also a possible precipitate above pH > 5.5 and some amorphous forms of $Al(OH)_3$ (i.e. Gibbsite) could also precipitate above pH 5 (Lozano et al., 2019a, 2019b, 2020a; Sánchez-España et al., 2011). Manganese containing mineral phases, such as birnessite ((Na, Ca)$Mn_7O_{14}$) and/or todorokite (($(Ca,Na,K)_xMn_6O_{12}$)) were also observed to precipitate along the alkalinization process (Hedin et al., 2019). Gypsum ($CaSO_4.2H_2O$) may precipitate regardless of the pH change along the alkalinization process due to the high concentrations of sulfate and Ca in the pore waters after calcite ($CaCO_3$) dissolution (Ferreira da Silva et al., 2009; Lozano et al., 2020a; Sánchez-España et al., 2011; Lozano et al., 2019b; Bortnikova et al., 2020). Schwertmannite, basaluminite and gypsum have been identified as the major secondary minerals precipitated inside the limestone-DAS PTS (Orden et al., 2021; Rotting et al., 2008). At the end, the treated AMD flowing out from such limestone-DAS PTS in the IPB has a pH value of around 6.5 and almost 100% removal of trivalent metals has been observed (Noack et al., 2014; Orden et al., 2021). Though divalent metals precipitation is favored above pH 8, the precipitation of Fe and Al containing secondary mineral phases have been shown to scavenge transition metals and arsenate (Ayora et al., 2016; Orden et al., 2021; Sánchez-España et al., 2011; Lozano et al., 2019b).

The AMDs can contain REE at concentration levels ranging between 4000 and 80,000 pmol/L (Ayora et al., 2016). The REE possess unique properties which make them technology critical elements (Ferreira da Silva et al., 2009; Ayora et al., 2013; Hassas et al., 2020; Royer-Lavallee et al., 2020; Los Elementos de las Tierras, 2015; Bau et al., 2018; Costis et al., 2021; Protano FR, 2002; Migaszewski and Gałuszka, 2014) and due to increased emissions into the environment (Ferreira da Silva et al., 2009; Perez-Lopez et al., 2011; Gonzalez et al., 2020; Soyol-Erdene et al., 2018; Costis et al., 2021; Protano FR, 2002; Migaszewski and Gałuszka, 2014; Gammons et al., 2005; Lozano et al., 2020b; Park et al., 2016; Prudencio et al., 2015; Sahoo et al., 2012; Sikakwe et al., 2018; Stolpe et al., 2013), REE are also considered as emerging contaminants. Hence scavenging them from AMD in a PTS for further recycling may be attractive, both to limit emissions in the environment and to provide more sustainable REE sources. Today there is a rather limited attention to the risks and mitigations of REE in AMD, likely because the environmental risk assessments of REE are still in their infancy. Studies showed that some PTS scavenged REE (Costis et al., 2021; Prudencio et al., 2015; Naidu et al., 2019). Several removal mechanisms, such as co-precipitation and/or sorption (i.e. surface complexation) can be responsible for this REE scavenge along the PTS (Ferreira da Silva et al., 2009; Lozano et al., 2020a; Sánchez-España et al., 2011; Lozano et al., 2019b). Though the number of studies remains limited, mapping techniques, such as synchrotron based μ-X-ray fluorescence (μXRF) and field emission scanning electron microscopy with energy-dispersive X-ray spectroscopy (FESEM-EDS) showed the potential retention of REE by Al-precipitates (i.e. basaluminite) in these systems (Ayora et al., 2016; Hedin et al., 2019).

There is an increasing attention in using alkaline waste materials in PTS to replace limestone, as it could improve the environmental footprint. Those materials represent economically and environmentally promising alternatives (Jones and Cetin, 2017; Millán-Becerro et al., 2021). Their use enables waste recycling leading to industrial symbiosis (Jones and Cetin, 2017). Nevertheless, it is important to achieve similar or better removal of contaminants present in AMD compared to the classical reagents for both heavy metals and REE. Examples of such waste materials are blast furnace slag (BFS) generated during smelting of iron ore in a blast furnace, and biomass ashes (BA) derived from combustion of biomass. The global annual production of BA is estimated to be 480 Mt and the bulk of it, as a primary management strategy, ends up in landfills (Millán-Becerro et al., 2021; Bogush et al., 2019). The global annual production of BFS exceeds 25 million Mt (Dzięcioł and Radziemska, 2022). Slag is usually used in road construction industry as an aggregate, however managing huge amounts of slag still remains a challenge (Dzięcioł and Radziemska, 2022). BFS and BA contain oxides that are not only a source of alkalinity, such as CaO, MgO and $K_2O$ but also contain amorphous and crystalline phases and thus reactive surfaces to which REE and transition metals can adsorb, i.e. these waste products may be superior alkaline materials compared to lime only, a hypothesis that still remains to be tested. Given the potential of BFS and BA to be used as alkaline materials in remediating AMD will allow recycling of those waste materials and hence handling of huge waste piles will no longer represent a problem. Moreover, it is important to better understand the mechanisms involved in REE removal using these waste materials. This would allow, if ever judged as an interesting prospect, to better design REE retrieval methods from PTS.

This study was set up to identify the efficiency of alkaline waste materials in remediating AMD and scavenging REE. The strategy was to compare the removal of REE and trace elements as a function of the BFS or BA dose with corresponding doses of limestone or NaOH, all at an equivalent near neutral pH (about 6.5). The $CaCO_3$, BFS and BA all contain Ca and will likely induce gypsum precipitation. To identify the effect of gypsum, pure NaOH was included as a reference material not containing Ca. The waste material and the formed secondary mineral phases were characterized by SEM-EDX, XRD and/or XRF to get some

insight into the REE immobilization mechanisms.

## 2. Materials and methods

### 2.1. Acid mine drainage sampling and characterization

The AMD used in the experiments was collected from a permanent leachate flowing out from a sulfide dump located in the NE of the Filon Norte open pit in the Tharsis mining area. The Tharsis mining area is located in the Huelva province (SW Spain) and is the second mine in importance of the IPB. This area is one of the most polluted in the IPB (Tornos et al.; GonzáLez et al., 2022; Moreno González et al., 2019; Santisteban et al., 2019; Valente et al., 2013) and most interesting for the purpose of the present study due to its high concentration of REE (Moreno González et al., 2019). The selected AMD is representative of extremely acid and metal-rich mining leachates of the Iberian Pyrite Belt and are characterized by seasonal variations with maximum concentrations of elements typically present in AMD in summer (dry period) and due to evaporation and lower ones in winter (wet period) due to dilution effect by rainfall. More details about seasonal variations of acid mine drainage from the Tharsis mines are given by Moreno-González et al. (2022) (Gonzalez et al., 2020). The AMD sample was collected at the end of April which is a representative of an intermediate period (between wet and dry period).

Field measurements were carried out at the sample location with a HACH sensION™ + MM150 portable multimeter probe to determine pH, electrical conductivity (EC), redox potential (ORP) and temperature. Before use, the electrodes were calibrated according to the manufacturer's instructions using certified materials. The AMD water sample was collected in pre-washed (10% $HNO_3$) polyethylene containers. An aliquot of the sample was filtered through a 0.22 μm PVDF membrane filter unit. A fraction was acidified with $HNO_3$ Suprapur to prevent metal precipitation and kept at 4 °C until analysis by Inductively Coupled Plasma Mass Spectrometry (ICP-MS) (Agilent 7700x ICP-MS) for its elemental composition (Fe, Al, transition metals and REE). A second filtered fraction was kept at 4 °C without acidification for subsequent anion analysis using Ion Chromatography IC (IC Dionex) and total organic and inorganic carbon content analysis using a TIC/TOC analyzer (Shimadzu TOC-L-CPH analyzer). The ultrapure water produced with a Milli-Q water purification system (Sartorius Water purific. SAR10) was used for necessary sample dilutions before any analysis. For the quality control of the method, blank samples, reference standards and duplicate analysis were used.

### 2.2. Alkaline waste materials

The BFS used in this study was obtained in powdered form from Ecocem Benelux B.V. (Netherlands). It is generated by smelting of iron ore in a blast furnace and subsequently dried and ground into a fine powder. The BA was obtained from a small power plant (50 MW) located in Huelva in Spain and operated by ENCE where over 500,000 tons of biomass is burnt annually for electricity production. BA was sieved to obtain homogenized sample (<63 μm). The two solids were characterized using different techniques including X-ray Fluorescence (XRF), Scanning Electron Microscopy coupled with an Energy Dispersive Spectroscopy (SEM/EDX) and X-ray diffraction (XRD). A Spectro XEPOS HE XRF was used to determine the elemental composition of BFS and BA. The analyses were performed on dried fine grinded (<250 μm) samples (±10 g each). A Phenom Desktop SEM equipped with an EDX device was used to observe the morphology and to identify the elemental composition of the waste materials. Before analysis, the solids were pressed into 1.3 cm sized pellets, mounted on aluminum stubs and coated with an ultrathin layer (5 nm) of gold to make their surfaces conductive. Imaging was done at a voltage of 10 kV, while EDX spot analyses targeting major phases were performed at an elevated voltage of 15 kV. The presence of crystalline phases in BFS and BA were determined by using XRD (Bruker D8 Advance) equipped with a Cu Kα source, a beam knife, a Ni filter and automated divergence slits. Operational settings were set at 40 kV and 40 mA and measurements were done between 5 and 60°2θ at a step size of 0.02°2θ. With the aim of quantitatively analyzing the mineral phases present, the powdered samples were mixed with 10 wt% of ZnO as internal standard. XRD measurements were then obtained using thin films of powder samples. Data semi-quantification was done using the Rietveld refinement method and the content of amorphous phases in each sample was calculated based on the use of ZnO as internal standard.

The acid neutralizing capacity (ANC) of BFS and BA was determined using pH titration. The definition of ANC depends on the selected final pH (Wahlström et al., 2009). Here, about 0.1–0.5 g of each waste material was mixed with 100 ml MilliQ water (initial pH of the solutions were around 9.6–9.9) and subsequently titrated with 0.1 M HCl (prepared by diluting Titrisol®) down to pH 6.5, each in duplicates. This pH was selected as a representative to what is usually achieved in limestone-DAS PTS in IPB. The ANC was calculated according to Equation (1).

$$Acid\ neutralizing\ capacity\ (ANC), mmol \Big/ kg = \frac{mmol\ H^+}{material, kg} \qquad \text{Equation 1}$$

With mmol $H^+$, the amount of $H^+$ added and the material in kg, the mass of solid titrated.

### 2.3. Batch alkalinization experiments

Preliminary batch alkalinization experiments were performed by adding different amounts of BA, BFS, analytical grade NaOH or $CaCO_3$ to the AMD solution to determine the quantity of each material to reach pH of ~6.5. In general, the intention of installing PTS is to achieve neutral pH in the treated water to fulfill the requirement imposed by the Food and Agriculture Organization of the United Nations (FAO) for irrigation waters. However, the PTS used in the Spanish part of the IPB being based on the DAS system are able to increase the pH only up to ≈ 6.5. Therefore, it was decided to raise the pH to ≈6.5 to compare the efficiencies of BFS and BA with $CaCO_3$. The solutions were shaken on an orbital shaker (Ohaus Orbital Shaker) under a constant speed for two weeks and pH was recorded. Based on that, final experiments were set up by mixing the required doses of alkaline materials (Table 1) to 20 mL AMD solution in 50 mL Nalgene tubes to raise the pH to ~6.5, each in duplicate. Suspensions after the addition of the alkaline materials were kept in the orbital shaker under a constant speed for two weeks to ensure proper contact between the added alkaline materials and the AMD solution. Based on the preliminary batch studies, this contact period was sufficient to achieve a stable pH. The precipitated solids and supernatants were subsequently collected after separation by centrifugation (Sigma 6-16 KS) at 7000×*g* for 10 min and the pH of the supernatants were measured using InLab Routine Pro probe (Mettler Toledo). The supernatants were then filtered at 0.22 μm on PVDF filter. A portion of the filtrates was acidified with 1% (V/V) $HNO_3$ (65% Suprapur, Merck) to avoid metal precipitation and analyzed by ICP-MS to obtain the final concentrations of Fe, Al and trace elements including REE. Another portion of the filtrates was analyzed by IC to obtain the final concentrations of sulfate.

The solids were freeze-dried (Telstar LyoQuest 85 Plus) before

**Table 1**
Required dose (alkaline material:AMD) ratio to increase pH to ~6.5 and the resulting pH.

| Alkaline material | pH | Dose (g/L) |
|---|---|---|
| NaOH | 6.43 ± 0.05 | 15 ± 0.18 |
| $CaCO_3$ | 6.47 ± 0.10 | 23 ± 0.10 |
| BFS | 6.67 ± 0.05 | 36 ± 0.03 |
| BA | 6.32 ± 0.10 | 185 ± 0.30 |

characterization. The morphology and the elemental analysis of the formed solid samples were characterized by SEM/EDX (Phenom Desktop) following the same sample preparation and analysis procedure as mentioned before. The identification and (semi)-quantification of the formed secondary phases were examined by XRD as described previously.

### 2.4. Thermodynamic modelling

The geochemical code PHREEQC (Parkhurst and Appelo, 2013) Interactive (version 3.6.2–15100) together with the thermodynamic database Thermoddem _v1.10 (Blanc et al., 2012) were used to calculate the saturation state of possible mineral phases in the AMD before and after alkalinization and the REE speciation in solution. The Thermoddem_v1.10 database (the activity model utilized is Bdot (Parkhurst and Appelo, 1999)) was chosen as it contains thermodynamic data for all REE. The database was complemented by the incorporation of thermodynamic data for the mineral phases schwertmannite and basaluminite found in literature. The respective equilibrium reactions and constants are shown in Table SI 1 in the supporting information.

According to Wood et al. (1990), REE di-sulfate complexes (i.e. $Ln(SO_4)_2^-$) become important when the sulfate concentration in solution containing REE is greater than 0.02 M (Wood, 1990). Therefore, the REE speciation of the AMD was performed after incorporating $Ln(SO_4)_2^-$ complexes in the ThermoddemV1.10 (TD) thermodynamic database (TDB) (Blanc et al., 2012). The thermodynamic data of the $Ln(SO_4)_2^-$ complexes (except for Ce) were integrated into the TDB from the Lawrence Livermore National Laboratory (LLNL) TDB (Spahiu and Bruno, 1995) by performing the required thermodynamic data conversions to keep consistency.

## 3. Results and discussion

### 3.1. Acid mine water

The pH of the AMD measured in the field was 1.8, confirming the severity of AMD pollution around the sample collection area. The low pH level is related to the extreme sulfuric acid concentrations (0.4 mol/L) (Table 2). The ORP of 397 mV indicates the oxidizing nature of this AMD and the EC value of 18.5 mS/cm reveals the presence of high concentrations of ions which is further confirmed by analysis of the AMD (Table 2). In addition to the high concentration of sulfate, the high concentrations of Fe, Al and Mn together with relatively high concentrations of other trace metals (i.e. Zn, Cu, Co, Ni, etc.) make AMD very toxic justifying the requirement for remediation (Ayora et al., 2016; Perez-Lopez et al., 2011; Lozano et al., 2020b; Reguer et al., 2020). The high concentrations of REY ($\sum$REY = 29 μmol/L) (Table 2) also confirms their increased mobilization in AMD related to the sulfide-sulfate oxidation processes.

**Table 2**
The concentration (<0.22 μm) of major, transition elements and REE measured by ICP-MS, $SO_4^{2-}$ measured by IC and TIC/TOC measured by TIC/TOC analyzer (Means and standard deviation; n = 2).

| Major elements and transition elements | | Rare earth and yttrium (REY) elements | |
|---|---|---|---|
| | mmol/L | | μmol/L |
| $SO_4^{2-}$ | 400 ± 20 | La | 2 ± 0.1 |
| Mg | 100 ± 5.1 | Ce | 6 ± 0.3 |
| Fe | 70 ± 3.2 | Pr | 0.8 ± 0.06 |
| Al | 40 ± 2.7 | Nd | 4 ± 0.2 |
| Ca | 10 ± 0.4 | Sm | 1 ± 0.06 |
| Na | 10 ± 0.6 | Eu | 0.3 ± 0.02 |
| Zn | 7 ± 0.3 | Gd | 2 ± 0.04 |
| Mn | 4 ± 0.1 | Tb | 0.2 ± 0.01 |
| Cu | 1 ± 0.6 | Dy | 1 ± 0.07 |
| Co | 0.2 ± 0.01 | Y | 10 ± 0.0 |
| Ni | 0.1 ± 0.01 | Ho | 0.2 ± 0.01 |
| As | 0.05 ± 0.0 | Er | 0.7 ± 0.03 |
| TIC | 0.02 ± 0.003 | Tm | 0.09 ± 0.00 |
| TOC | 0.2 ± 0.07 | Yb | 0.5 ± 0.03 |
| | | Lu | 0.07 ± 0.01 |

According to the respective limit values recommended by the FAO for irrigation waters (Ayers and Westcot, 1985), the concentrations of Fe, Al, Mn, Cu, Zn and sulfates in this AMD are 811, 266, 1146, 574, 233 and 65 times higher, respectively. Therefore, impelled firstly by the European Water Framework Directive (Moreno-Gonzalez et al., 2022), and the urgent need of water for agricultural activities, there is a plan to remediate the catchment around this area (Lozano et al., 2020b).

The concentrations of REE in AMD normalized to European Shale (EUS) show an upward convex curvature shaped pattern suggesting Middle REE (MREE) enrichment in this AMD (Fig. 1). In fact, the ratios of $Er_N/Gd_N$ and $Gd_N/La_N$ were < 1 and > 1, respectively which confirmed this enrichment. The MREE enrichment is a common feature of such AMD (Ayora et al., 2016; Prudencio et al., 2015; Sahoo et al., 2012) and is due to the preferential release of MREE from MREE enriched minerals such as monazite, apatite (e.g. phosphates) and bastnasite (e.g. carbonates in the host rock under acidic conditions. (Prudencio et al., 2015; León et al., 2023).

Geochemical modelling of saturation states revealed undersaturation of schwertmannite upon four different $K_s$ commonly used in literature (schwertmannite1-4: see Table SI 2 in the supporting information),as well as ferrihydrite, basaluminite and gibbsite in the AMD before alkalinization. The SI of Gypsum was however close to zero, meaning thus close to equilibrium (Table SI 2). Therefore, gypsum seems to control aqueous sulfate concentration in the AMD.

The calculated REE speciation in the AMD is shown in Figure SI 1. It is clear that REE mono-sulfate complexes (i.e. $LnSO_4^+$) are the dominating species in the AMD for most of the REE. Yet, REE di-sulfate complexes $Ln(SO_4)_2^-$ are also shown to be important species in this AMD in agreement with the 0.02 M sulfate concentration threshold stated by Wood (1990). Moreover, small percentages of free REE species (i.e. $Ln^{3+}$) are also predicted to be present in the AMD.

Further modelling about the alkalinization experiments was done and will be discussed in the respective result and discussion section (under section 3.3).

### 3.2. Alkaline materials

The elemental composition of BFS and BA obtained from X-ray fluorescence analysis are presented in Table 3.

The BFS is mostly composed of Ca and Si containing phases. According to the literature, BFS usually has a $CaO/SiO_2$ ratio of

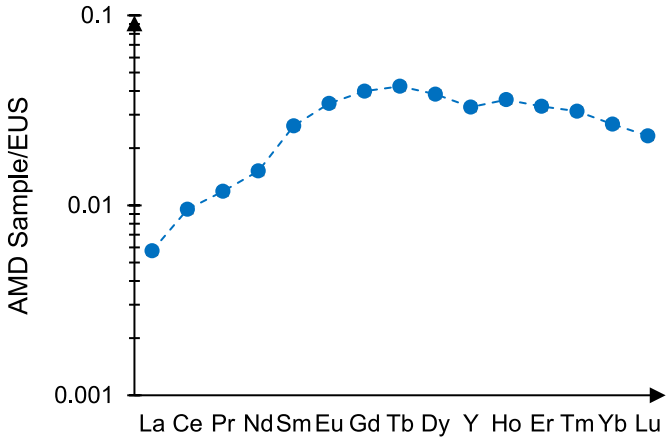


**Fig. 1.** Normalized REE concentrations (<0.22 μm) with respect to European Shale (Means and standard deviation; n = 3).

**Table 3**
Percent oxide composition of BFS and BA using XRF.

| % | $Na_2O$ | MgO | $Al_2O_3$ | $SiO_2$ | $K_2O$ | CaO | $Fe_2O_3$ | $TiO_2$ |
|---|---|---|---|---|---|---|---|---|
| BFS | 0.8 | 8.6 | 9.9 | 38.5 | 0.4 | 40.6 | 0.5 | 0.6 |
| BA | 3.1 | 3.9 | 11.3 | 53.8 | 4.4 | 18.3 | 4.4 | 0.7 |

approximately 1, which is consistent with the value measured here, i.e. 1.1 (Simmons et al., 2014). Moreover, nearly 95% of the total slag is usually composed primarily of $SiO_2$, $Al_2O_3$, CaO and MgO, which is also the case here (97%) (Dzięcioł and Radziemska, 2022; Simmons et al., 2014). BFS is usually defined as a calcium aluminosilicate rich waste due to presence of this combination of elements and oxides (Fayed et al., 2021). BA is mostly composed of Si followed by Ca which is consistent with the XRD mineralogical information mentioned below (Table 5). Unlike BFS, BA usually has a variable composition (Bogush et al., 2019). The Vassilev's chemical classification mentioned in (Bogush et al., 2019) can be used to identify the type of ash and its level of acid tendency (the ability to release $H^+$ ions in aqueous solution), which is useful to evaluate the efficiency of ashes to remediate AMD (Bogush et al., 2019). According to that classification, BA used in this study belongs to the siliceous CaO rich ash with medium acid tendency (SC-MA type) which is in fact good for AMD remediation (Bogush et al., 2019). This is confirmed by the ANC of BFS and BA at pH 6.5 shown in Table 4. The ANC of BFS and BA mainly comes from the dissolution of Ca, Mg, K and Na contained in the (amorphous) phases therein (Table 3). The BFS has ~2 times higher ANC than BA, which is consistent with the higher content of basic oxides in BFS (~50%) as compared to BA (~30%).

The XRD results presented in Table 5 show that BFS is mainly composed of amorphous mineral phases and small quantities of calcite and merwinite [$Ca_3Mg(SiO_4)_2$]. The BA is mainly comprised of amorphous phases and quartz. In addition, plagioclase feldspar [(Na,Ca)(Si,Al)$_4O_8$] and calcite were also identified in BA. The respective XRD spectra are shown in the supplementary information (Figure SI 3). Calcite is present in both BFS and BA and is thus contributing to the alkaline generating capacity. Merwinite which is a commonly found mineral in slag comprises also Ca and Mg and upon dissolution at acidic pH may also contribute to the alkaline generating capacity of BFS (Engström et al., 2013). However, this effect can be considered minor/negligible as the present merwinite content in BFS is very small compared to the other phases therein. This is also true for plagioclase feldspar in BA (OXBURGH et al., 1994). In addition, these amorphous and crystalline phases could serve as sorbing surfaces for REE and transition metals.

The morphology of BFS and BA examined using SEM and by their elemental composition measured using EDX are shown in Fig. 2. The SEM images show that BFS and BA mainly consist of irregular-shaped particles with diameters up to 30 μm. The EDX confirms the total elemental analyses: BFS mainly composes of Ca, Si, Al, Mg as major elements with some S as impurity. The presence of oxygen in the EDX results indicates the presence of oxides as well. Silica in BFS is present as amorphous $SiO_2$ rather than quartz, which is not present based on the XRD analysis. The BA consists of Si, Ca, Al, K and Fe as major elements with Mg and Na as impurities.

### 3.3. Batch alkalinization experiments

The doses required to raise the pH of AMD to pH = 6.5 ranked BA > BFS > $CaCO_3$ > NaOH (Table 1) and are in line with the inverse of the ANC of these products (Table 4). The theoretical ANC to pH 6.5 of $CaCO_3$ and NaOH are 20,000 mmol/kg (or 10,000 mmol/kg if only dissolves to $HCO_3^-$ and no $CO_2$ escapes) and 25,000 mmol/kg, respectively.

**Table 4**
Acid neutralizing capacity of BFS and BA (Means and standard deviation; n = 2).

| | ANC down to pH 6.5, mmol $H^+$/kg |
|---|---|
| **BFS** | 504 ± 3.0 |
| **BA** | 264 ± 4.2 |

**Table 5**
Semi-quantitative XRD analysis of BFS and BA.

| Wt % | Merwinite [$Ca_3Mg(SiO_4)_2$] | Calcite [$CaCO_3$] | Plagioclase (Na, Ca feldspar) [(Na, Ca)(Si,Al)$_4O_8$] | Quartz [$SiO_2$] | Amorphous |
|---|---|---|---|---|---|
| **BFS** | 0.7 | 0.3 | 0 | 0 | 99 |
| **BA** | 0 | 2.6 | 3.5 | 24 | 70 |

The % removal of sulfate after the alkalinization experiments with the four different alkaline materials is shown in Table 6. The most effective sulfate removal is achieved by using $CaCO_3$, while the least effective sulfate removal is observed when using NaOH. This result is consistent with the Ca content of the alkaline materials and their capacity to induce gypsum precipitation. The BFS and BA remove equal fractions of sulfate even though they do not have the same Ca content.

According to the FAO standards for irrigation waters (Ayers and Westcot, 1985), the residual sulfate concentration should not exceed 5.2 × $10^{-3}$ mol/L. None of the alkaline materials was able to reach that standard because none of these have a sufficiently soluble Ca. This was also the case after the limestone-DAS PTS at the Mine Esperanza in the IPB in which a residual sulfate concentration of 2.1 × $10^{-2}$ mol/L (around a 30% sulfate removal) was present (Orden et al., 2021). This implies the need for additional treatment for removal sulfates. Studies showed that the use of $BaCO_3$-DAS system as an additional unit after the limestone-DAS was promising in this regard, i.e. increased the sulfate removal via the precipitation of $BaSO_4$ (Gomez-Arias et al., 2015; Torres et al., 2018). Alternatively, speciation calculations show that more sulfate can be precipitated as gypsum using $CaCl_2$ as a source of soluble $Ca^{2+}$.

It should be noted that, however, a direct comparison is not possible with the limestone-DAS system installed in the field because of the difference between the $CaCO_3$ that was used in this study and the natural limestone that is being used in the field (i.e. DAS system together with woodchips). Though the matrixes are different, the trends obtained from this study are similar to the ones in the "real" limestone-DAS system.

The batch alkalinization experiments were simulated by using the initial AMD composition (Table 2) and experimental doses of $CaCO_3$ and NaOH (Table 1) as reactants with gypsum added as a secondary phase as it is the dominating phase precipitation during AMD alkalinization. Fe- and Al- phases (schwertmannite and basaluminte) precipitation were not taken into account as at this stage it is not certain which type of schwertmannite or basaluminite have been precipitated and thus having no constraint for the simulations. Alkalinization path was represented by hundred calculation steps and the reaction step that matched best with the measured pH was used to estimate the amount of gypsum precipitation. This was done with the intention of obtaining rough calculation to assess gypsum precipitation. However, more detailed modelling will be done in the future considering already compiled thermodynamic data of Fe- and Al- phases (schwertmannite and basaluminte).

The alkalinization of the AMD/pH is mainly related to $CaCO_3$ dissolution (related to $H^+$ consumption) (Table SI 3) while the precipitation of Fe- and Al- oxyhydroxysulfates are associated to $H^+$ release (Table SI 3). Gypsum precipitation is also contributing to $H^+$ consumption (Table SI 3). Therefore, the precipitation of Fe- and Al- oxyhydroxysulfates may play a role in buffering the pH of the system and also in the sulfate precipitation during AMD alkalinization.

Batch reaction calculations predict that $CaCO_3$ addition to reach pH 6.5, results in gypsum precipitation (~1.8 × $10^{-1}$ mol/L). Mass balance calculations reveal that however ~50% (about 1.8 × $10^{-1}$ mol/L) of sulfate still remain in solution. This amount is slightly higher than the measured residual sulfate (Table 6). In the experiments using NaOH, the

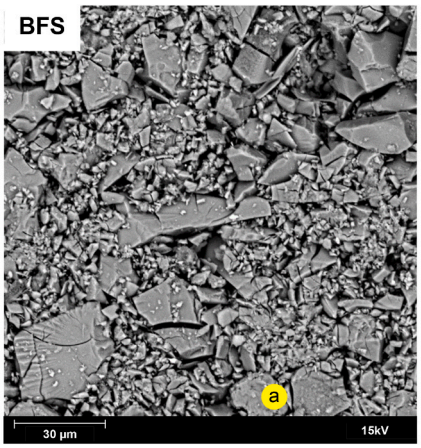


a

| Element | Atomic % | Weight % |
|---|---|---|
| O | 66.06 | 49.50 |
| Ca | 12.18 | 22.86 |
| Si | 11.54 | 15.18 |
| Al | 5.19 | 6.56 |
| Mg | 4.55 | 5.18 |
| S | 0.48 | 0.72 |

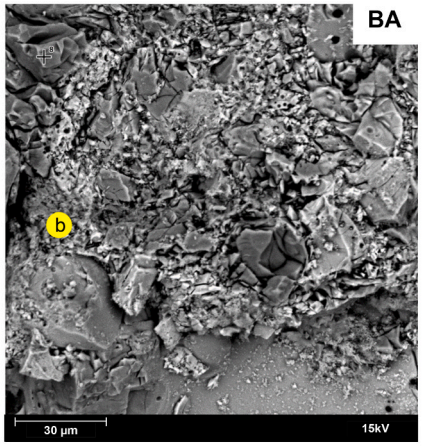


b

| Element | Atomic % | Weight % |
|---|---|---|
| O | 57.91 | 39.62 |
| Si | 20.1 | 24.13 |
| Ca | 6.67 | 11.42 |
| Al | 6.08 | 7.02 |
| K | 4.59 | 7.68 |
| Fe | 3.93 | 9.40 |
| Mg | 0.46 | 0.48 |
| Na | 0.25 | 0.24 |

**Fig. 2.** SEM images of BFS and BA with the elemental composition as measured by EDX.

**Table 6**
residual sulfate concentration and % removal of sulfate after the alkalinization (Means and standard deviation; n = 2).

| | Residual sulfate concentration, mol/L | Removal of sulfate [%] |
|---|---|---|
| **NaOH** | 0.27 ± 0.03 | 19 ± 4 |
| **$CaCO_3$** | 0.13 ± 0.03 | 62 ± 3 |
| **BFS** | 0.16 ± 0.02 | 54 ± 2 |
| **BA** | 0.16 ± 0.01 | 54 ± 2 |

geochemical calculations predict precipitation of only $3.1 \times 10^{-3}$ mol/L of gypsum, logically leading to a higher residual sulfate concentration (about $3.6 \times 10^{-1}$ mol/L), which is slightly higher than the measured one (Table 6). In both cases the slightly higher calculated residual sulfate concentrations can be attributed to the fact that sulfate containing Fe- and Al-phases were not considered in the calculations. No geochemical calculations were done for BFS and BA, as their exact compositions are not known and no thermodynamic data are available for these materials. The reactions referred to in the text above (occurring during alkalinization) are given in Table SI 3.

The XRD analysis showed that the precipitated solids after the alkalinization experiments mainly consist of amorphous phases, irrespective of the alkaline material used (Table 7). The respective XRD spectra are provided in the supplementary information (Figure SI 4).

**Table 7**
(Mineral) composition of the precipitates after the experiment using XRD characterization.

| Alkaline agent | wt% | | | |
|---|---|---|---|---|
| | Amorphous | Gypsum | Quartz | Calcite |
| **NaOH** | 100 | – | – | – |
| **$CaCO_3$** | 72 | 18 | – | 9 |
| **BFS** | 64 | 36 | – | – |
| **BA** | 76 | 3 | 21 | – |

Only amorphous phases precipitated in the NaOH treated solutions. The XRD results clearly show gypsum precipitation during $CaCO_3$, BFS and BA alkalinization which is attributed to the Ca in the added alkaline materials. The lowest sulfate removal obtained with NaOH (Table 6) can therefore be explained by the absence of gypsum precipitation during this alkalinization as indicated by the XRD analysis. The other crystalline phases observed by XRD after BA and $CaCO_3$ alkalinization, i.e., quartz and calcite, respectively, correspond most likely to the primary quartz and calcite present in the unreacted materials.

The SEM images of the samples after alkalinization using the four different alkaline materials are shown in Fig. 3. The Ca, S and O rich phases correspond to gypsum minerals with characteristic elongated shapes and are visible in the treatments with $CaCO_3$ (denoted by the spots of d and f), with BFS (denoted by the spots of h and i) and with BA (denoted by the spots of k and m) but are not visible with NaOH. These results are in agreement with XRD results (Table 7). Moreover, Fe, Al, S and O rich phases which are not clearly crystalline were common with all four different alkaline materials: NaOH (denoted by the spots of a, b and c), $CaCO_3$ (denoted by the spots of e and g), BFS (denoted by the spot of j) and BA (denoted by the spots of n and l). Therefore, the amorphous phases identified by XRD should mainly be composed of Fe, Al, S and O rich phases i.e., Fe and Al-containing oxyhydroxysulfates. The spots of a, b, c, e, g, j, l and n contain trace amounts of Zn while the spots of b, e and n contains trace amounts of Cu as well. This indicates Zn and Cu removal along with those Fe, Al, S and O rich phases precipitation. None of the REE-concentrations was detectable with SEM/EDX.

### 3.3.1. *Metal removal*

The residual concentrations of Al, Mn, Fe, Cu and Zn remaining in solution after the alkalinization are shown in Fig. 4.

The lowest residual Al concentration of $2.7 \times 10^{-5}$ mol/L is obtained after alkalinization with BA, whereas the highest residual Al concentration of $8.0 \times 10^{-5}$ mol/L is measured after alkalinization with NaOH. The residual Al concentrations using $CaCO_3$ and BFS are similar, i.e., $4.0 \times 10^{-5}$ mol/L. Thus, BA yields a better Al removal than BFS. Overall, all

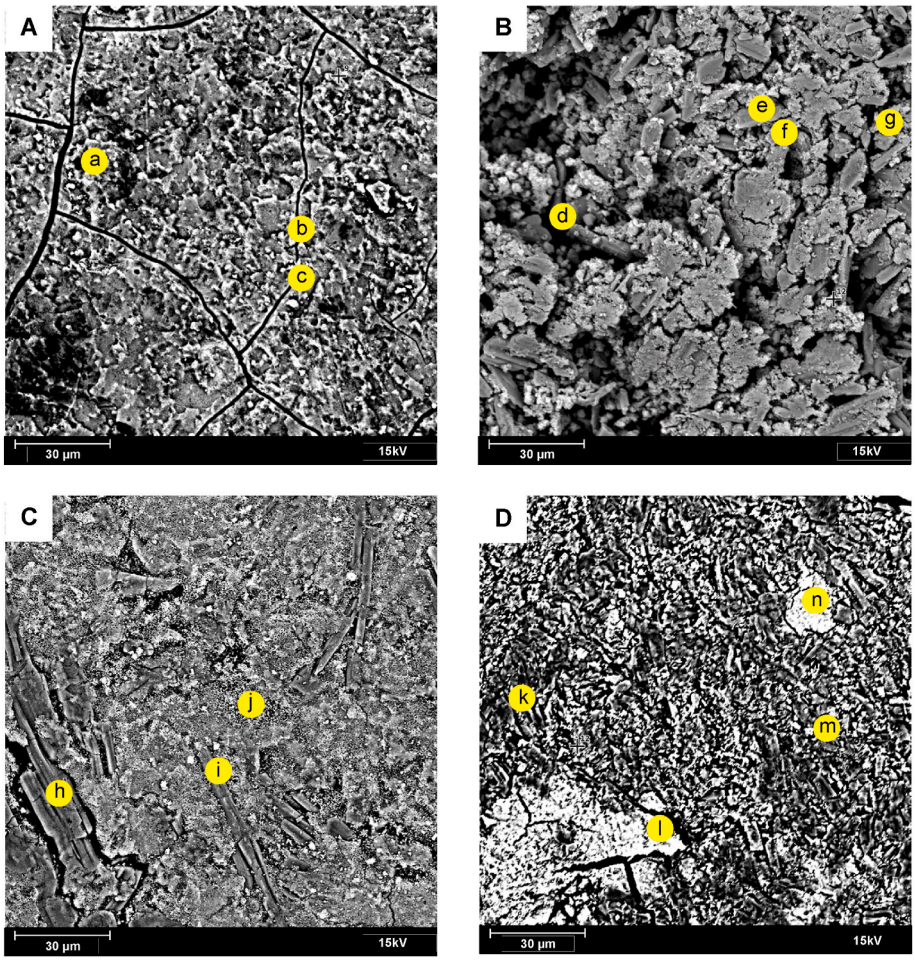


**Fig. 3.** SEM images of samples after the alkalinization experiments with NaOH: A; $CaCO_3$: B; BFS: C and BA: D.

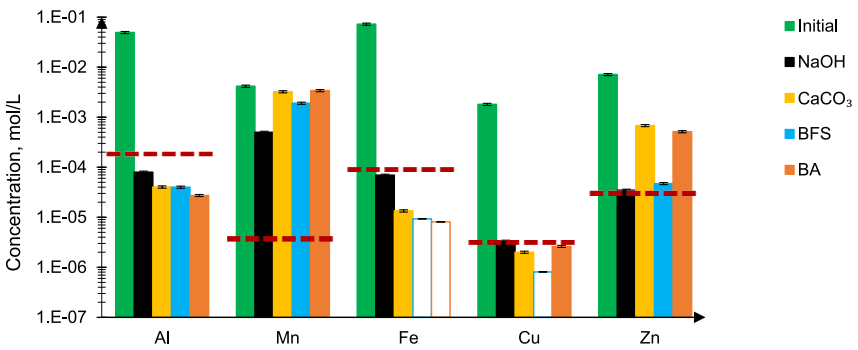


**Fig. 4.** Initial and residual concentrations of Al, Mn, Fe, Cu and Zn. (Dashed lines indicate the respective FAO irrigation waters standards (Ayers and Westcot, 1985); Unfilled bars: detection limit. Measured concentrations were below that limit. Means and standard deviation (n = 2 after treatment and n = 3 before treatment).

four materials show above 99.8% removal of Al after the alkalinization which represents an efficient remediation of the initial AMD. Moreover, alkalinization using all four materials were able to meet the criteria of the FAO for irrigation water. According to literature, for the treated AMD flowing out of the limestone-DAS PTS at the Mine Esperanza abandoned mine, a residual concentration of $3.7 \times 10^{-6}$ mol/L was achieved (Orden et al., 2021). This is better than what is obtained after $CaCO_3$ alkalinization during our experiments. Yet, it is noteworthy that the PTS at the Esperanza Mine consists of two successive limestone-DAS reactors to improve its performances (Orden et al., 2021).

The residual concentration of Fe after the alkalinization with NaOH and $CaCO_3$ corresponds respectively to $6.9 \times 10^{-5}$ mol/L and $1.3 \times 10^{-5}$ mol/L. The residual Fe concentration with BFS is less than $9.3 \times 10^{-6}$ mol/L, while with BA it is less than $8.1 \times 10^{-8}$ mol/L, which accounts for more than 99.9% Fe removal. The Al and Fe comprised in the materials did not increase the concentration of these elements in

solution, the residual concentrations of these two elements were even lower in BA and BFS treatments compared to $CaCO_3$ and NaOH. Similar to Al, alkalinization using all four materials were also able to comply with the recommended value given in the FAO for irrigation water for Fe (i.e., $8.95 \times 10^{-5}$ mol/L). Fe removal efficiency during the first limestone DAS unit at the Esperanza Mine was only 49.5%. This lower Fe removal efficiency is attributed to the presence of Fe mainly as $Fe^{2+}$ in that AMD which required an additional oxidation step to convert $Fe^{2+}$ to $Fe^{3+}$ for a better removal of Fe.

Over 99% removal of Cu and above 90% removal of Zn are achieved by all four alkaline materials. The removal of Mn however was lower compared to the Cu and Zn removal. The lowest residual concentration of Cu after the alkalinization is achieved with BFS ($<8.1 \times 10^{-7}$ mol/L) while the lowest residual concentration of Zn and Mn are achieved using NaOH ($3.3 \times 10^{-5}$ mol/L and $5.0 \times 10^{-4}$ mol/L respectively) closely followed by BFS. Comparatively, better removal of Cu, Zn and Mn are achieved with BFS than with BA. This could be due to better sorption of those contaminants onto the surface of the BFS and on the precipitated mineral phases. With respect to the DAS PTS systems, a 92.6% Cu removal and around 80.4% Zn removal were achieved in the first limestone-DAS reactive tank at the Esperanza Mine treatment unit (Orden et al., 2021). The FAO limits for irrigation water of Cu, Zn and Mn should be $3.15 \times 10^{-6}$ mol/L, $3.06 \times 10^{-5}$ mol/L and $3.64 \times 10^{-6}$ mol/L, respectively. For Cu, all alkaline materials except NaOH comply with this reference value. Yet, none of the used alkaline materials allowed to meet with residual Zn and residual Mn value indicated in FAO for irrigation water. However, it is noteworthy that the residual Zn concentration after NaOH and BFS alkalinization are not far from the limit. The higher mobility of Mn in AMD treatments in comparison with other metals such as Cu and Zn has been previously reported (Orden et al., 2021). Additional treatment step(s) would therefore be required to improve such divalent metal removal. A multi-step alkaline PTS has been proposed with the use of MgO-DAS preceded by limestone-DAS to facilitate the increase of pH above 10 and thereby to achieve a better removal of divalent metals including Mn (Macias et al., 2012b).

Given the fact that above 99.9% of Fe and above 99.8% of Al are removed from the AMD, the formed solids should definitely contain Fe and Al, which is consistent with the SEM data. The precipitation of amorphous to poorly crystalline schwertmannite, i.e., a Fe containing oxyhydroxysulfate and basaluminite, an Al containing oxyhydroxysulfate are reported in the literature. (Sánchez-España et al., 2011; Protano FR, 2002; Lozano et al., 2020b; Park et al., 2016). This is also consistent with what is reported for the DAS PTS in the IPB (Orden et al., 2021). Geochemical modelling revealed that some forms of schwertmannite were still over-saturated in the supernatants after alkalinization with NaOH and $CaCO_3$ (Table SI 4). This indicates those phases did not reach equilibrium yet in the supernatant and thus could be still in the process of precipitation. However, schwertmannite_2 after alkalinization with NaOH and schwertmannite_4 after alkalinization with $CaCO_3$ were closer to equilibrium (Table SI 4). None of the Fe phases were predicted after alkalinization with BFS and BA as the respective Fe concentrations were below LoQ (Table SI 4). Similar to the schwertmannites, two forms of basaluminite were also over-saturated in the supernatants after alkalinization regardless of the alkaline material used (Table SI 4) indicating those forms could also still be precipitating. Nevertheless, gibbsite (amorphous) phase was slightly oversaturated in all the supernatants indicating the possibility of Al hydroxides precipitation instead of Al oxyhydroxysulfates precipitation. The removal of the divalent metals, i.e., Cu and Zn, is likely due to co-precipitation/sorption with/on Fe and Al containing secondary mineral phases (Lozano et al., 2019b, 2020c; Caraballo et al., 2011). Cánovas et al. (2020) reported that Cu and Zn may be associated with basaluminite precipitation during AMD alkalinization with limestone.

Comparatively, BA is more efficient for Fe and Al removal while BFS is more efficient for divalent metal removal as revealed by the residual concentrations in the supernatants after alkalinization. This could be due to a slightly higher pH at the end of BFS alkalinization (pH 6.67) than that after BA alkalinization (pH 6.32). Yet, overall both BFS and BA perform as good as, if not better than the currently used limestone and appear as good replacement options. However, the FAO for irrigation water criteria is not all met with these materials. Thus, additive treatment units like for example $BaCO_3$-DAS and MgO-DAS should be considered (Gomez-Arias et al., 2015; Torres et al., 2018; Macias et al., 2012b).

### 3.3.2. REE removal after alkalinization

The calculated REE speciation in the supernatants after alkalinization is shown in Figure SI 2. It revealed that around pH 6.5, REE carbonated complexes ($LnCO_3^+$) could also be present in addition to the $LnSO_4^+$, $Ln(SO_4)_2^-$ and $Ln^{3+}$. The percentage of $LnCO_3^+$ is the largest in the supernatant after alkalinization with $CaCO_3$ among others while it is the lowest in the supernatant after alkalinizaiton with NaOH.

Fig. 5 presents the initial and residual concentrations of the REE.

Overall, REE removal is effective with all four alkaline materials used (>99.7%). These REE removal efficiencies are higher than what has been obtained in the field after the first limestone-DAS pond (i.e. 97.3%) at the Mina Esperanza mine (Orden et al., 2021). Contrary to transition metals, there are yet no REE limits. With respect to residual REE concentrations, alkalinization with $CaCO_3$ yields lowest residual REE concentrations while the highest residual REE concentrations are obtained with NaOH alkalinization. On average across all REE, residual REE are factor 2.5 higher in NaOH treatment than in the mean of BA, BFS and $CaCO_3$. The removal of LREE is less efficient compared to MREE and HREE with all four alkaline materials. The residual LREE concentrations follow the order of $CaCO_3$<BFS < BA < NaOH, whereas residual MREE concentrations follow the order of BFS < BA < $CaCO_3$<NaOH. Meanwhile the residual HREE concentrations follow the order of BA < BFS < $CaCO_3$<NaOH. Previous studies have suggested that REE removal during AMD alkalinization in limestone-DAS PTS is mainly due to co-precipitation with Al containing secondary mineral phases (i.e., basaluminite) (Orden et al., 2021). Moreover, other studies showed also sorption of REE on Fe and Al mineral phases (above pH 5 on basaluminite (Lozano et al., 2019b) and above pH 6.5 on schwertmannite (Lozano et al., 2020a)). Gypsum may also be a host for scavenging REE which is suggested by the clearly lower removal efficiency obtained with NaOH, where gypsum was not formed, in comparison to the other alkaline materials. The ionic radius of $Ca^{2+}$ in gypsum structure (in 8-fold coordination) is very similar to those of REE, there is indeed a possibility - especially for LREE - to fit into the gypsum structure as $LREE^{3+}$ (Table SI 5). Such incorporation process was indeed identified by several researchers (Dutrizac, 2017; Lin et al., 2019; Sadri et al., 2018, 2019). It would therefore be worth investigating further the role of gypsum in REE scavenging during AMD alkalinization.

In reality, PTS work on longer time scales. Therefore, ageing might also have an influence on the long-term retention of REE, i.e. incorporation or release from the structure with crystallization (Sánchez-España et al., 2011). Further studies using advanced characterization techniques (i.e., synchrotron-based techniques) and ageing experiments are needed for the confirmation of the retention mechanisms of REE.

## 3.4. Environmental and economic implications

Based on our results, the two tested waste materials are shown to perform as efficiently in remediating AMD and in retaining REE as commercial reagents. However, the amount of solid needed for an efficient neutralization of the AMD when using such waste materials, is higher than with $CaCO_3$ and NaOH. This is especially true for BA, which required in the current experiments eight times the amount of $CaCO_3$ and five times the amount of BFS to reach pH 6.5. One could argue that the need for a higher amount of solid would be a drawback in terms of transport and logistic perspective. However, with respect to environmental aspects, “recycling" BFS/BA in PTS support industrial symbiosis

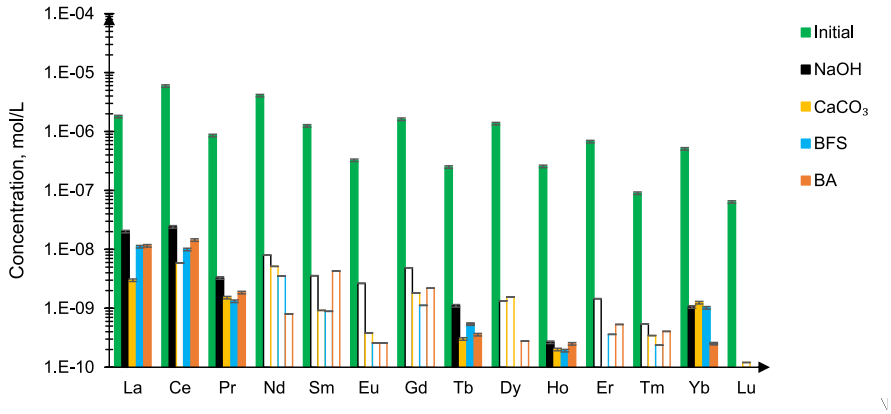


**Fig. 5.** The initial concentrations of REE and the residual concentrations of REE after the alkalinization experiments (Unfilled bars: detection limit. Measured concentrations were below that limit. Means and standard deviation (n = 2 after treatment and n = 3 before treatment).

and also circular economy. In fact, such associated transport and logistic costs could offset the costs associated with using commercial reagents and disposing of BFS/BA otherwise considered as waste. The DAS PTS at the Esperanza Mine alone used close to 25 tons of calcite per year which is close to around 1 million Euro per year (Orden et al., 2021; Millán-Becerro et al., 2021). The entire Tharsis mining area in the IPB contains approximately 5.2 $hm^3$ of acidic water (Moreno González et al., 2019). Assuming AMD composition to be the same around the entire area, use of calcite as alkaline material is associated with more than 11 million Euro (considering the market price of 90–100 euro per ton).

Moreover, the possibility to retrieve critical elements of economic interest, such as REE from the solid precipitates, which still remains to be evaluated, would further help in offsetting the associated transport and logistic costs in using such waste materials improving the sustainability of such AMD PTS. This option has been proved suitable (Macías et al., 2017) using dilute commercial acids.

## 4. Conclusions

This study focused on comparing two different alkaline waste materials, i.e. BFS and BA with the classical alkaline agents $CaCO_3$ and NaOH for the remediation of highly acidic and metal rich AMD sampled in the IPB.

Based on the ANC determination and on the quantity of material needed to neutralize the pH of the AMD samples, it was found that BFS has a higher neutralizing capacity than BA, thus requiring less BFS addition than BA to reach a new neutral pH (pH = 6.5). Nevertheless, higher amounts of both materials are required for alkalinization as compared to the classical reagents $CaCO_3$ and NaOH.

Overall, the two tested waste materials showed good potential for the remediation of AMD from the IPB. Both materials were efficiently able to neutralize the AMD and to remove Fe, Al and heavy metals. The Al and Fe comprised in the waste materials did not impend the remediation and the concentration of these two elements. They even decreased in the remediated solutions as compared to their concentrations after alkalinization with $CaCO_3$ and NaOH.

With respect to their efficiency in removing REE, all four alkaline materials showed above 99.7% removal. However, with respect to the residual REE concentrations, the lowest were achieved using $CaCO_3$ for alkalinization. Both BFS and BA can be considered as efficient REE remediating agents with a better performance of BFS. Indirect evidence suggest that gypsum may be a host for scavenging REE. The requirement for higher amounts of BFS and BA than using $CaCO_3$ for efficient remediation of the AMD could be viewed as beneficial in terms of environmental point of view. The associated transport and logistic costs of using such waste materials could be offset by 1) associated economic costs of using commercial materials such as calcite and 2) associated economic benefits from being able to retrieving critical elements of economic interest such as REE. Further studies however are required for a correct estimation and confirmation of the latter. All those combined would improve the sustainability of AMD PTS leading to industrial symbiosis and thus circular economy.

The overall poorer performance of NaOH in remediating AMD in comparison to the other tested materials, highlighted that the efficiency of remediation is not only a matter of alkalinization but also of the type of the precipitated phases. The presence of Ca in the alkaline material allowing gypsum precipitation was clearly shown to enhance the removal of heavy metals and REE. Yet, a lot of open questions remain to be answered on the exact nature of removal mechanism(s) along the alkalinization process occurring inside PTS, especially for REE. Many removal mechanisms, such as co-precipitation, sorption (i.e. surface complexation) - alone or combined - could be responsible for the REE scavenge. Unravelling the fate of REE along the passive treatment system would therefore pave a path to enhance the concentration of REE in the precipitated solids for subsequent recovery at a later stage.

## Declaration of competing interest

The authors declare that they have no known competing financial interests or personal relationships that could have appeared to influence the work reported in this paper.

## Data availability

Data will be made available on request.

## Acknowledgments

This research has received funding from European Union's Horizon 2020 research and innovation program under the Marie Sklodowska-Curie Grant Agreement No 857989. C.R Cánovas thanks the Spanish Ministry of Science and Innovation for the Postdoctoral Fellowship granted under application reference RYC2019-027949-I.

The authors gratefully acknowledge the valuable assistance of the following people as well: Dr. Raul Moreno Gonzalez from the Department of Earth Sciences, University of Huelva in Spain for assistance in collecting acid mine water samples; Dr. Quoc Tri Phung from SCK CEN in Belgium for assistance in obtaining BFS samples; Dr. Lander Frederickx from SCK CEN in Belgium for supporting in XRD analysis; Dr. Claudia Moens, Mr. Benoit Bergen and Ms. Kristin Coorevits, ICP-MS Team, Division of Soil and Water management, KU Leuven for their enormous assistance in measuring ICP-MS samples; All the technicians of the Waste and Disposal Group, SCKCEN for their assistance in various ways. Authors also thank ENCE Energía y Celulosa Company for

providing the BA.

## Appendix A. Supplementary data

Supplementary data to this article can be found online at https://doi.org/10.1016/j.apgeochem.2023.105800.

## List of abbreviations

| | |
|---|---|
| AMD | Acid Mine Drainage |
| REE | Rare Earth Elements |
| BFS | Blast Furnace Slag |
| BA | Biomass Ashes |
| IPB | Iberian Pyrite Belt |
| ATS | Active Treatment Systems |
| PTS | Passive Treatment Systems |
| DAS | Dispersed Alkaline Substrate |
| μXRF | μ-X-ray fluorescence |
| FESEM-EDS | Field Emission Scanning Electron Microscopy with Energy-Dispersive X-ray Spectroscopy |
| EC | Electrical Conductivity |
| ORP | Oxidation Reduction Potential |
| ICP-MS | Inductively Coupled Plasma Mass Spectrometry |
| IC | Ion Chromatography |
| TIC/TOC | Total Inorganic Carbon/Total Organic Carbon |
| SEM/EDX | Scanning Electron Microscopy/Energy Dispersive Spectroscopy |
| XRD | X-ray Diffraction |
| ANC | Acid Neutralization Capacity |
| TD | ThermoddemV1.10 |
| TDB | Thermodynamic Database |
| LLNL | Lawrence Livermore National Laboratory |
| REY | Rare Earth Elements and Yttrium |
| EUS | European Shale |
| LREE | Light Rare Earth Elements |
| MREE | Middle Rare Earth Elements |
| HREE | Heavy Rare Earth Elements |
| FAO | Food and Agriculture Organization of the United Nations |
| LoQ | Limit of Quantification |

## References


Akinwekomi, V., Kefeni, K.K., Maree, J.P., Msagati, T.A.M., 2016. Integrated acid mine drainage treatment using Mg(OH) 2 or Mg(HCO3)2 and Ca(OH)2: implications for separate removal of metals and sulphate. Int. J. Miner. Process. 155, 83–90.

Ayers, R.S., Westcot, D.W., 1985. Water Quality for Agriculture Rome Food and Agriculture Organization of the United Nations.

Ayora, C., Caraballo, M.A., Macias, F., Rotting, T.S., Carrera, J., Nieto, J.M., 2013. Acid mine drainage in the Iberian Pyrite Belt: 2. Lessons learned from recent passive remediation experiences. Environ. Sci. Pollut. Res. Int. 20 (11), 7837–7853.

Ayora, C., Macias, F., Torres, E., Lozano, A., Carrero, S., Nieto, J.M., et al., 2016. Recovery of rare earth elements and yttrium from passive-remediation systems of acid mine drainage. Environ. Sci. Technol. 50 (15), 8255–8262.

Bau, M., Schmidt, K., Pack, A., Bendel, V., Kraemer, D., 2018. The European Shale: an improved data set for normalisation of rare earth element and yttrium concentrations in environmental and biological samples from Europe. Appl. Geochem. 90, 142–149.

Ben Ali, H.E., Neculita, C.M., Molson, J.W., Maqsoud, A., Zagury, G.J., 2019. Performance of passive systems for mine drainage treatment at low temperature and high salinity: a review. Miner. Eng. 134, 325–344.

Bernier, L.R., 2005. The potential use of serpentinite in the passive treatment of acid mine drainage: batch experiments. Environ. Geol. 47 (5), 670–684.

Blanc, P., Lassin, A., Piantone, P., Azaroual, M., Jacquemet, N., Fabbri, A., et al., 2012. Thermoddem: ageochemical database focused on low temperature water/rock interactions and waste materials. Appl. Geochem. 27, 2107–2116.

Bogush, A.A., Dabu, C., Tikhova, V.D., Kim, J.K., Campos, L.C., 2019. Biomass ashes for acid mine drainage remediation. Waste and Biomass Valorization 11 (9), 4977–4989.

Bortnikova, S., Gaskova, O., Yurkevich, N., Saeva, O., Abrosimova, N., 2020. Chemical treatment of highly toxic acid mine drainage at A gold mining site in southwestern siberia, Russia. Minerals 10 (10).

Cánovas, C.R., Nieto, J.M., Macías, F., Basallote, M.D., Olías, M., Pérez-López, R., et al., 2020. Recovery of critical raw materials from acid mine drainage (AMD). In: Elvis Fosso-Kankeu, C.W., Burgess, Jo (Eds.), Recovery of Byproducts from Acid Mine Drainage Treatment. Wiley.

Caraballo, M.A., Rötting, T.S., Macías, F., Nieto, J.M., Ayora, C., 2009. Field multi-step limestone and MgO passive system to treat acid mine drainage with high metal concentrations. Appl. Geochem. 24 (12), 2301–2311.

Caraballo, M.A., Macias, F., Rotting, T.S., Nieto, J.M., Ayora, C., 2011. Long term remediation of highly polluted acid mine drainage: a sustainable approach to restore the environmental quality of the Odiel river basin. Environ. Pollut. 159 (12), 3613–3619.

Costis, S., Mueller, K.K., Coudert, L., Neculita, C.M., Reynier, N., Blais, J.-F., 2021. Recovery potential of rare earth elements from mining and industrial residues: a review and cases studies. J. Geochem. Explor. 221.

Doye, I., Duchesne, J., 2003. Neutralisation of acid mine drainage with alkaline industrial residues: laboratory investigation using batch-leaching tests. Appl. Geochem. 18 (8), 1197–1213.

Duraes, N., Bobos, I., da Silva, E.F., 2017. Speciation and precipitation of heavy metals in high-metal and high-acid mine waters from the Iberian Pyrite Belt (Portugal). Environ. Sci. Pollut. Res. Int. 24 (5), 4562–4576.

Dutrizac, J.E., 2017. The behaviour of the rare earth elements during gypsum (CaSO 4 ·2H 2 O) precipitation. Hydrometallurgy 174, 38–46.

Dzięcioł, J., Radziemska, M., 2022. Blast furnace slag, post-industrial waste or valuable building materials with remediation potential? Minerals 12 (4).

Engström, F., Adolfsson, D., Samuelsson, C., Sandström, Å., Björkman, B., 2013. A study of the solubility of pure slag minerals. Miner. Eng. 41, 46–52.

Fayed, E.K., El-Hosiny, F.I., El-Kattan, I.M., Abdel-Gawwad, H.A., 2021. An Innovative Method for the Sustainable Utilization of Blast-Furnace Slag in the Cleaner Production of One-Part Hybrid Cement. Research Square.

Ferreira da Silva, E., Bobos, I., Xavier Matos, J., Patinha, C., Reis, A.P., Cardoso Fonseca, E., 2009. Mineralogy and geochemistry of trace metals and REE in volcanic massive sulfide host rocks, stream sediments, stream waters and acid mine drainage from the Lousal mine area (Iberian Pyrite Belt, Portugal). Appl. Geochem. 24 (3), 383–401.

Gammons, C.H., Wood, S.A., Pedrozo, F., Varekamp, J.C., Nelson, B.J., Shope, C.L., et al., 2005. Hydrogeochemistry and rare earth element behavior in a volcanically acidified watershed in Patagonia, Argentina. Chem. Geol. 222 (3–4), 249–267.

Gomez-Arias, A., Castillo, J., Welman-Purchase, M., Posthumus, J., van Heerden, E. (Eds.), 2015. Evidences of Effective Treatment of Alkaline Mine Drainage with BaCO3. 10th International Conference of Acid Rock Drainage and IMWA Annual Conference. Santiago de Chile).

Gonzalez, R.M., Canovas, C.R., Olias, M., Macias, F., 2020. Rare earth elements in a historical mining district (south-west Spain): hydrogeochemical behaviour and seasonal variability. Chemosphere 253, 126742.

GonzáLez, F., Moreno, C., SáEz, R., Clayton, G., 2022. Ore genesis age of the tharsis mining district (iberian pyrite Belt): a palynological approach. J. Geol. Soc. 159 (3), 229–232.

Hassas, B.V., Rezaee, M., Pisupati, S.V., 2020. Precipitation of rare earth elements from acid mine drainage by CO2 mineralization process. Chem. Eng. J. 399, 11.

Hedin, B.C., Capo, R.C., Stewart, B.W., Hedin, R.S., Lopano, C.L., Stuckman, M.Y., 2019. The evaluation of critical rare earth element (REE) enriched treatment solids from coal mine drainage passive treatment systems. Int. J. Coal Geol. 208, 54–64.

Hengen, T.J., Squillace, M.K., O'Sullivan, A.D., Stone, J.J., 2014. Life cycle assessment analysis of active and passive acid mine drainage treatment technologies. Resour. Conserv. Recycl. 86, 160–167.

Jones, S.N., Cetin, B., 2017. Evaluation of waste materials for acid mine drainage remediation. Fuel 188, 294–309.

León, R., Macías, F., Cánovas C, R., Pérez-López, R., Ayora, C., Nieto, J.M., et al., 2021. Mine waters as a secondary source of rare earth elements worldwide: the case of the Iberian Pyrite Belt. J. Geochem. Explor. 224.

León, R., Macías, F., Cánovas C, R., Millán-Becerro, R., Pérez-López, R., Ayora, C., et al., 2023. Evidence of rare earth elements origin in acid mine drainage from the Iberian Pyrite Belt (SW Spain). Ore Geol. Rev. 154.

Lin, J., Nilges, M.J., Wiens, E., Chen, N., Wang, S., Pan, Y., 2019. Mechanism of Gd3+ uptake in gypsum (CaSO4·2H2O): implications for EPR dating, REE recovery and REE behavior. Geochem. Cosmochim. Acta 258, 63–78.

Los Elementos de las Tierras Raras, 2015. Huelva.

Lozano, A., Fernandez-Martinez, A., Ayora, C., Di Tommaso, D., Poulain, A., Rovezzi, M., et al., 2019a. Solid and aqueous speciation of yttrium in passive remediation systems of acid mine drainage. Environ. Sci. Technol. 53 (19), 11153–11161.

Lozano, A., Ayora, C., Fernández-Martínez, A., 2019b. Sorption of rare earth elements onto basaluminite: the role of sulfate and pH. Geochem. Cosmochim. Acta 258, 50–62.

Lozano, A., Ayora, C., Fernández-Martínez, A., 2020a. Sorption of rare earth elements on schwertmannite and their mobility in acid mine drainage treatments. Appl. Geochem. 113.

Lozano, A., Ayora, C., Macías, F., León, R., Gimeno, M.J., Auqué, L., 2020b. Geochemical behavior of rare earth elements in acid drainages: modeling achievements and limitations. J. Geochem. Explor. 216.

Lozano, A., Ayora, C., Fernandez-Martinez, A., 2020c. Sorption of Rare earth elements on schwertmannite and their mobility in acid mine drainage treatments. Appl. Geochem. 113, 104499.

Macias, F., Caraballo, M.A., Nieto, J.M., Rotting, T.S., Ayora, C., 2012a. Natural pretreatment and passive remediation of highly polluted acid mine drainage. J. Environ. Manag. 104, 93–100.

Macias, F., Caraballo, M.A., Rotting, T.S., Perez-Lopez, R., Nieto, J.M., Ayora, C., 2012b. From highly polluted Zn-rich acid mine drainage to non-metallic waters:

implementation of a multi-step alkaline passive treatment system to remediate metal pollution. Sci. Total Environ. 433, 323–330.
Macías, F., Pérez-López, R., Caraballo, M.A., Cánovas, C.R., Nieto, J.M., 2017. Management strategies and valorization for waste sludge from active treatment of extremely metal-polluted acid mine drainage: a contribution for sustainable mining. J. Clean. Prod. 141, 1057–1066.
Masindi, V., 2017. Recovery of drinking water and valuable minerals from acid mine drainage using an integration of magnesite, lime, soda ash, CO2 and reverse osmosis treatment processes. J. Environ. Chem. Eng. 5 (4), 3136–3142.
Migaszewski, Z.M., Gałuszka, A., 2014. The characteristics, occurrence, and geochemical behavior of rare earth elements in the environment: a review. Crit. Rev. Environ. Sci. Technol. 45 (5), 429–471.
Millán-Becerro, R., Cánovas, C.R., Pérez-López, R., Macías, F., León, R., 2021. Combined procedure of metal removal and recovery of technology elements from fertilizer industry effluents. J. Geochem. Explor. 221.
Moreno González, R., Olías, M., Cánovas, C.R., Macías, F. (Eds.), 2019. Acid Mine Drainage Pollution at the Tharsis Mines (Iberian Pyrite Belt): A Serious Environmental and Socioeconomic Problem. IMWA 2019 "Mine Water: Technological and Ecological Challenges".
Moreno-Gonzalez, R., Macias, F., Olias, M., Ruiz Canovas, C., 2022. Temporal evolution of acid mine drainage (AMD) leachates from the abandoned tharsis mine (Iberian Pyrite Belt, Spain). Environ. Pollut. 295, 118697.
Naidu, G., Ryu, S., Thiruvenkatachari, R., Choi, Y., Jeong, S., Vigneswaran, S., 2019. A critical review on remediation, reuse, and resource recovery from acid mine drainage. Environ. Pollut. 247, 1110–1124.
Ness, I., Janin, A., Stewart, K., 2014. Passive Treatments of Mine Imapacted Water in Cold Climates: A Review. Yukon Research Centre, Yukon College.
Noack, C.W., Dzombak, D.A., Karamalidis, A.K., 2014. Rare earth element distributions and trends in natural waters with a focus on groundwater. Environ. Sci. Technol. 48 (8), 4317–4326.
Orden, S., Macias, F., Canovas, C.R., Nieto, J.M., Perez-Lopez, R., Ayora, C., 2021. Eco-sustainable passive treatment for mine waters: full-scale and long-term demonstration. J. Environ. Manag. 280, 111699.
Oxburgh, R., Drever, J.I., Sun, Y.-T., 1994. Mechanism of plagioclase dissolution in acid solution at 25°C. Geochem. Cosmochim. Acta 58 (2), 661–669.
Park, J.H., Han, Y.S., Ahn, J.S., 2016. Comparison of arsenic co-precipitation and adsorption by iron minerals and the mechanism of arsenic natural attenuation in a mine stream. Water Res. 106, 295–303.
Parkhurst, D.L., Appelo, C.A.J., 1999. User's Guide to PHREEQC (Version 2): A Computer Program for Speciation, Batch-Reaction, One-Dimensional Transport, and Inverse Geochemical Calculations. U.S. Geological Survey.
Parkhurst, D.L., Appelo, C.A.J., 2013. Description of Input and Examples for PHREEQC Version 3–a Computer Program for Speciation, Batch-Reaction, One-Dimensional Transport, and Inverse Geochemical Calculations. Reston, Virginia.
Perez-Lopez, R., Macias, F., Caraballo, M.A., Nieto, J.M., Roman-Ross, G., Tucoulou, R., et al., 2011. Mineralogy and geochemistry of Zn-rich mine-drainage precipitates from an MgO passive treatment system by synchrotron-based X-ray analysis. Environ. Sci. Technol. 45 (18), 7826–7833.
Protano FR, G., 2002. High contents of rare earth elements (REEs) in stream waters of a Cu–Pb–Zn mining area. Environ. Pollut. 117, 499–514.
Prudencio, M.I., Valente, T., Marques, R., Sequeira Braga, M.A., Pamplona, J., 2015. Geochemistry of rare earth elements in a passive treatment system built for acid mine drainage remediation. Chemosphere 138, 691–700.
Reguer, S., Kergourlay, F., Foy, E., Neff, D., Vantelon, D., Cotte, M., et al., 2020. XANES at the Cl K-edge as a relevant technique to reveal the iron archaeological artefact dechlorination treatments. J. Anal. Atomic Spectrom. 35 (10), 2358–2368.
Rotting, T.S., Thomas, R.C., Ayora, C., Carrera, J., 2008. Passive treatment of acid mine drainage with high metal concentrations using dispersed alkaline substrate. J. Environ. Qual. 37 (5), 1741–1751.
Royer-Lavallee, A., Neculita, C.M., Coudert, L., 2020. Removal and potential recovery of rare earth elements from mine water. J. Ind. Eng. Chem. 89, 47–57.
Ruehl, M.D., Hiibel, S.R., 2020. Evaluation of organic carbon and microbial inoculum for bioremediation of acid mine drainage. Miner. Eng. 157.
Sadri, F., Kim, R., Yang, Z., Ghahreman, A., 2018. The effect of calcium sulfate crystallization and the crystal modification on aqueous REE stability in Ca saturated REE-Ca-SO4-H2O systems. Hydrometallurgy 182, 82–96.
Sadri, F., Kim, R., Ghahreman, A., 2019. Substitution of calcium with Ce, Nd, Er, and Tb in the structure of microcrystals of calcium sulfates with controlled hydration water: a proposed mechanism. Cryst. Growth Des. 19 (5), 2621–2631.
Sahoo, P.K., Tripathy, S., Equeenuddin, S.M., Panigrahi, M.K., 2012. Geochemical characteristics of coal mine discharge vis-à-vis behavior of rare earth elements at Jaintia Hills coalfield, northeastern India. J. Geochem. Explor. 112, 235–243.
Sánchez-España, J., Yusta, I., Schwertmannite, Diez-Ercilla M., hydrobasaluminite, 2011. A re-evaluation of their solubility and control on the iron and aluminium concentration in acidic pit lakes. Appl. Geochem. 26 (9–10), 1752–1774.
Santisteban, M., Viers, J., Sarmiento, A.M., Grande, J.A., Luís, A.T., de la Torre, M.L., et al., 2019. Proposal of precipitation–dissolution models in a channel affected by acid mine drainage in the Iberian Pyrite Belt during torrential rain regimes. SN Appl. Sci. 1 (8).
Sheoran, A.S., 2006. Performance of three aquatic plant species in bench-scale acid mine drainage wetland test cells. Mine Water Environ. 25, 23–36.
Sheridan, G., Harding, K., Koller, E., De Pretto, A., 2013. A comparison of charcoal- and slag-based constructed wetlands for acid mine drainage remediation. WaterSA 39 (3).
Sikakwe, G.U., Otele, A., Ozibo, B.N., 2018. Chemical speciation and complexation modeling of trace and rare earth elements in groundwater of Oban Massif and Mamfe mMbayment southeastern Nigeria. Chem. Speciat. Bioavailab. 30 (1), 86–98.
Simmons, J., Ziemkiewicz, P., Courtney Black, D., 2014. Use of steel slag leach beds for the treatment of acid mine drainage. Mine Water Environ. 21 (2), 91–99.
Skousen, J.G., Ziemkiewicz, P.F., McDonald, L.M., 2019. Acid mine drainage formation, control and treatment: approaches and strategies. Extr. Ind. Soc. 6 (1), 241–249.
Soyol-Erdene, T.O., Valente, T., Grande, J.A., de la Torre, M.L., 2018. Mineralogical controls on mobility of rare earth elements in acid mine drainage environments. Chemosphere 205, 317–327.
Spahiu, K., Bruno, J., 1995. A Selected Thermodynamic Database for REE to Be Used in HLNW Performance Assessment Exercises. . MBT Tecnologia Ambiental. SWEDISH NUCLEAR FUEL AND WASTE MANAGEMENT CO, Cerdanyola, Spain.
Stolpe, B., Guo, L., Shiller, A.M., 2013. Binding and transport of rare earth elements by organic and iron-rich nanocolloids in Alaskan rivers, as revealed by field-flow fractionation and ICP-MS. Geochem. Cosmochim. Acta 106, 446–462.
Tornos F, López Pamo E, Sánchez España FJ. THE IBERIAN PYRITE BELT. p. 57-64..
Torres, E., Lozano, A., Macías, F., Gomez-Arias, A., Castillo, J., Ayora, C., 2018. Passive elimination of sulfate and metals from acid mine drainage using combined limestone and barium carbonate systems. J. Clean. Prod. 182, 114–123.
Totsche, O., Fyson, A., Kalin, M., Steinberg, C.E., 2006. Titration curves: a useful instrument for assessing the buffer systems of acidic mining waters. Environ. Sci. Pollut. Res. Int. 13 (4), 215–224.
Turingan, C.O.A., Cordero, K.S., Santos, A.L., Tan, G.S.L., Tabelin, C.B., Alorro, R.D., et al., 2022. Acid mine drainage treatment using a process train with laterite mine waste, concrete waste, and limestone as treatment media. Water 14 (7).
Valente, T., Grande, J.A., de la Torre, M.L., Santisteban, M., Cerón, J.C., 2013. Mineralogy and environmental relevance of AMD-precipitates from the tharsis mines, iberian pyrite Belt (SW, Spain). Appl. Geochem. 39, 11–25.
Wahlström, M., Laine-Ylijoki, J., Kaartinen, T., Bendz, OHoD., 2009. Acid Neutralization Capacity of Waste – Specification of Requirement Stated in Landfill Regulations. TemaNord, Copenhagen.
Wang, Y., Noble, A., Vass, C., Ziemkiewicz, P., 2021. Speciation of rare earth elements in acid mine drainage precipitates by sequential extraction. Miner. Eng. 168.
Wood, S.A., 1990. The aqueous geochemistry of the rare-earth elements and yttrium. Chem. Geol. 82, 159–186.
Zänker, H., Richter, W., Hüttig, G., 2003. Scavenging and immobilization of trace contaminants by colloids in the waters of abandoned ore mines. Colloids Surf. A Physicochem. Eng. Asp. 217 (1–3), 21–31.